ENERGY TRANSFERS ACROSS AN INTERNAL WAVE /VORTICAL MODE SPECTRUM

Dave Ramsden, Daleth Research, 1255 Oscar St. Victoria BC, V8V2X6 Canada

Greg Holloway, Institute of Ocean Sciences, Sidney, BC, V8L4B2 Canada

ABSTRACT

Nonlinear interactions among internal gravity waves are investigated by direct numerical experiments. In the first part of this paper, cases which solve the full (3D) Navier-Stokes equations are compared to cases in which variability is suppressed in one horizontal direction. It is found that the 3D and 2D simulations exhibit certain similarities. We find both in 3D and in 2D that the transfer of kinetic energy (KE) from large to small scales is less efficient than the transfer of potential energy (PE). The imbalance between these transfers leads to a characteristic buoyancy flux spectrum which is negative (KE to PE) at large scales and positive (PE to KE) at small scales. Integrated over all scales, the buoyancy flux is very small for a wide range of flow regimes. However, results concerning buoyancy flux are sensitive to assumptions about the manner of energetic forcing.

These sensitivities are taken up in the second part of the paper where energy is introduced in a 'surface' layer and removed via a bottom absorption layer. It is found that it is kinetic energy which is radiated down the fluid column and the mechanism for the radiation is the divergence of the pressure-velocity correlation. For these cases, buoyancy flux in the radiated region is on average negative. The buoyancy flux spectra, however, retain the same tendency to become positive at the smallest scales.

Energy balances in the radiation region for both kinetic and potential energy are shown to be qualitatively achieved between transport, buoyancy flux and dissipation terms without the need to posit a 'mean shear' extraction term. Buoyancy flux is shown to be of the same order as dissipation rate of kinetic or potential energy. Kinetic and potential energy dissipation rates are about equal.

INTRODUCTION

The objectives of this study are to attempt to determine the role of nonlinear transfers in the evolution of internal waves near dissipation scales. The first part of this work follows a paper recently submitted; *Ramsden and Holloway* [1990] (hereafter RH) on statistically homogeneous forced cases, so we will be mainly emphasizing the highlights of those investigations. The second part of this study is on surface layer forcing. This work is new and still under active investigation. In the spirit of 'Aha, we present the preliminary results.

Part 1: STATISTICALLY HOMOGENEOUS FORCED CASES

The starting point for RH was to attempt to isolate the effects of nonlinearities in the evolution of internal waves. In addition, they also wanted to consider the role of the zero frequency, potential vorticity containing component of the motion field [*Holloway*, 1983], the so called vortical mode [*Muller et al., 1988*]. Interaction of the vortical mode with the internal wave field is not well understood. In particular, the role of nonlinear interactions in rearranging wave and vortical energies at order 1–50 m scales is unknown. RH were also interested in determining the effects of nonlinear interactions on other flow parameters such as buoyancy flux and what effect restriction of the 3D motion field to vertical planar 2D would have.

There are two reasons to compare 2D results to 3D. The first is that it may be useful to run 2D simulations because the range of accessible scales is greater for given computer capacity. If the results are qualitatively similar to 3D, a great deal of time and effort can be saved by performing 2D simulations. The second reason is to ask what part(s) of the results from 2D theoretical treatments of internal waves may be applicable to the full 3D problem.

RH summarizes and follows up on numerical experiments reported in *Shen and Holloway* [1986] (non-rotating statistically stationary 2D internal waves), *Ramsden and Holloway* [1987] (2D with rotation), and *Holloway and Ramsden* [1988] (initial presentation of 3D results).

METHOD

The governing equations are the 3D nondimensionalized Navier-Stokes equations under the Bousinesq approximation;

$$\partial_t \mathbf{u} + \mathbf{u}\cdot\nabla\mathbf{u} = -\nabla p - \rho\mathbf{e}_z + \nu\nabla^2\mathbf{u} - 2\boldsymbol{\Omega}\times\mathbf{u} + \mathbf{F_u} \tag{1}$$

$$\partial_t \rho - W + \mathbf{u}\cdot\nabla\rho = \kappa\nabla^2\rho + F_\rho \tag{2}$$

$$\nabla\cdot\mathbf{u} = 0 \tag{3}$$

In (1) to (3), $\mathbf{u}$ is velocity (U,V,W) on basis vectors $(\mathbf{e_x}, \mathbf{e_y}, \mathbf{e_z})$, ∇ is the gradient operator, p is pressure, ρ is the departure from a mean background gradient of density, $\overline{\rho}$, ν is kinematic viscosity, $\boldsymbol{\Omega}$ is the earth's angular velocity, set to (0,0,f/2), $\mathbf{F_u}$ and F_ρ are external forcing, and κ is mass diffusivity. Time has been scaled such that the bv frequency $N = \left(\frac{g}{\rho_0}\frac{\partial\overline{\rho}}{\partial z}\right)^{1/2}$ (g gravity, ρ_0 reference density) is unity. Vorticity is defined to be $\Lambda=\nabla\times\mathbf{u}$. (1) to (3) are the equations employed by *Riley et al* [1981] in the pioneering study of 3D stratified turbulence, with the addition of rotation and forcing terms. Full details of the nondimensionalization may be found in *Riley et al.*

Spatial derivatives are calculated by the spectral transform method after *Orszag* [1971] in which each variable $\mathbf{u}, \rho$, etc. is expressed as a truncated Fourier series, a procedure which implies

periodic boundary conditions. On wavevectors $\mathbf{k} = (k_x, k_y, k_z)$ denote the Fourier transform of any field $a(\mathbf{x})$ to be $a_\mathbf{k}$:

$$\mathbf{u}(\mathbf{x}) = \sum_{\mathbf{k}} \mathbf{u}_\mathbf{k} e^{\iota \mathbf{k}\cdot\mathbf{x}} \tag{4}$$

$$\rho(\mathbf{x}) = \sum_{\mathbf{k}} \rho_\mathbf{k} e^{\iota \mathbf{k}\cdot\mathbf{x}} \tag{5}$$

A centered leapfrog method with a *Robert* [1966] filter to suppress the leapfrog mode was used to timestep the equations.

The 2D Analog

If the prognostic variables are subjected to the constraint that $\partial_x = 0$, the equations of motion can be written:

$$\partial_t \zeta + J(\psi, \zeta) - f\partial_z U + \partial_y \rho = F_\zeta + \nu\nabla^2\zeta \tag{6}$$

$$\partial_t \rho + J(\psi, \rho) - \partial_y \psi = F_\rho + \kappa\nabla^2\rho \tag{7}$$

$$\partial_t U + J(\psi, U) + f\partial_z \psi = F_U + \nu\nabla^2 U \tag{8}$$

With the planar velocities u= (V, W) given by streamfunction ψ, $V = -\partial_z\psi$, $W = \partial_y\psi$. Also, $\zeta = \Lambda \cdot \mathbf{e_x} = \nabla^2\psi$ and J is the nonlinear operator $J(A, B) = \partial_z A \cdot \partial_y B - \partial_y A \cdot \partial_z B$. Forcing takes the same form as the 3D simulations.

Notes on the Simulations: The Problem of Forcing

The 3D runs were performed at grid resolution 32^3 and the 2D simulations were performed at 128^2. These modest resolutions were chosen in order to be able to obtain statistically stationarity states and subsequent adequate averaging periods for a number of flow regimes. In both cases, suites of experiments were performed at Kolmogorov dissipation scales chosen to be the smallest resolvable scale $1/n$ where n is the number of grid points and the Kolmogorov scale is defined as $(\nu^3/\epsilon)^{\frac{1}{4}}$, where ϵ is the kinetic energy dissipation rate per unit volume or area $\epsilon = -\nu\mathbf{u}\cdot\nabla^2\mathbf{u}$. The Prandtl number ν/κ was unity for all cases.

So far, the form of the forcing has not been specified. The major problem is that due to limited computer storage, the forced scales are not well separated from the (Kolmogorov) dissipation scale. This will necessarily mean that results will be influenced by the form of the forcing. It

would be desirable to introduce energy at GM levels, but the requisite scales are much larger than those available to the model. At scales close to dissipation, there is some evidence for velocity isotropy [*Gargett et al* 1981]. Also, *Muller et al* [1988] infer significant vortical mode energy near dissipation (order 10m-1m) scales. For the purposes of this study, it was decided to take as a constraint a maximum entropy principle where kinetic and potential energies are forced in a 2:1 ratio (inviscid equipartition ratio) with all fields forced isotropically.

The forcing functions, *F(k)* were chosen to have energy spectra of

$$E[F(k)] = \frac{k^3}{(k^2 + k_0^2)^6} \tag{9}$$

for both 3D and 2D kinetic and potential energies; *ko* was given the value 7.

$$F(k) = A\sqrt{k}/(k^2 + 7^2)^3 \ (for\ 3D) \tag{10}$$

$$F(k) = Ak/(k^2 + 7^2)^3 \ (for\ 2D) \tag{11}$$

with A's amplitude factors. At each timestep in the running of the models, (10) and (11) were multiplied by a random phase factor, $e^{i\theta}$, $0 < \theta \leq 2\pi$. Kinetic and potential energy were forced in a 2:1 energy ratio and a separate random phase was chosen at each timestep with the proviso that the forcing of the 3D velocity field be nondivergent. The forcing function above has a maximum at wavenumber 4. It provides the criteria of being large scale, isotropic and forces KE:PE at energy equipartition rates. It also excites wave and vortical modes (see the section on waves and vortices).

The basic range of the experiments covered ratios of nonlinear to linear timescales as characterized by an r.m.s. turbulence Froude number (bv frequency, N, was unity) In 3D this is defined as $\sqrt{(\frac{\partial U}{\partial z})^2 + (\frac{\partial V}{\partial z})^2}$. In the 2D simulations, Froude number is defined as $\sqrt{(\frac{\partial V}{\partial z})^2}$, the achievement of a particular Froude number meant adjusting A and ν until statistically stationary states at the desired Froude numbers and Kolmogorov scales were reached whereupon time integrations of many Brunt-Vaisala periods were performed in order to calculate average statistics.

Figure 1a shows instantaneous density slices from 3D simulations at r.m.s. turbulence Froude numbers of 0.1, 0.3, 1 and 3. Figure 1b shows the same Froude numbers for 2D. These 4 cases are chosen to span the flow regimes likely to be encountered in the ocean, from weakly wavelike to strongly overturning. The cases presented in Figure 1 are without rotation. It may be seen from Figure 1 that overturning has begun by an r.m.s Froude number of about 1 for both 2D and 3D.

Table 1 gives some of the relevant parameters for the runs shown in Figure 1. The weaknesses of the direct simulations are seen in that for the 3D cases, the Reynold's numbers $|u|l/\nu$ based on the Taylor microscale

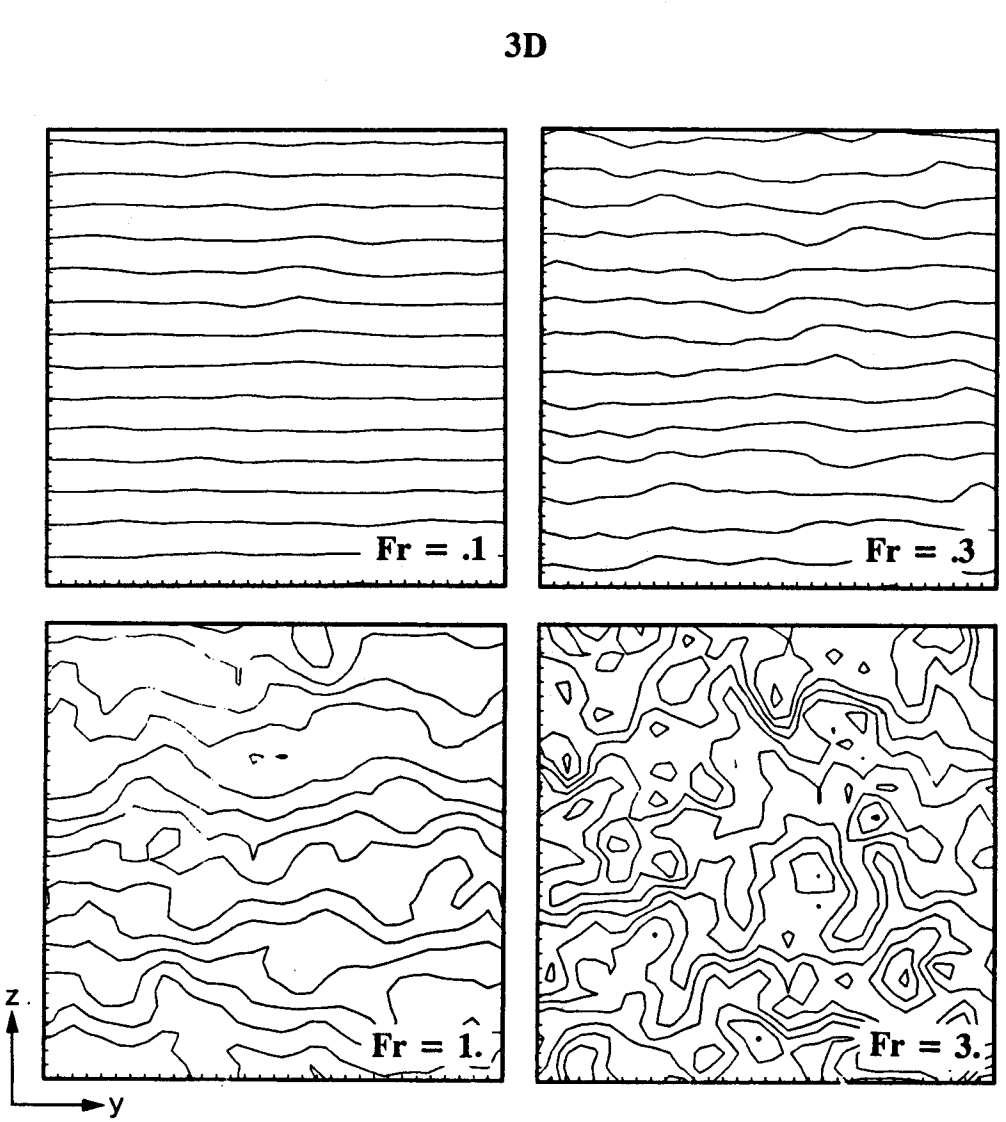

Figure 1a: Instantaneous density slices for (left to right, top to bottom), r.m.s. turbulence Froude numbers (Fr) of 0.1, 0.3, 1 and 3 for the 3D cases, all with f=0

$$l = \sqrt{\frac{15|u|^2}{|\Lambda|^2}} \tag{12}$$

are around 15–25. Any other measure of turbulent 'activity' indicates a highly viscous regime. Box sizes are small with all simulations near dissipation scales. On the other hand, the small flow domain justifies the use of a constant background gradient of density. Highly turbulent patches in a stratified environment are frequently of vertical size 10 m or less (e.g. *Moum* [1989]). Also, the measure of kinetic energy residence time KE/ϵ for the 3D Froude number 1 case is around 0.33 bv, which compares favorably with oceanic turbulence measurements [*Crawford*, 1987] .

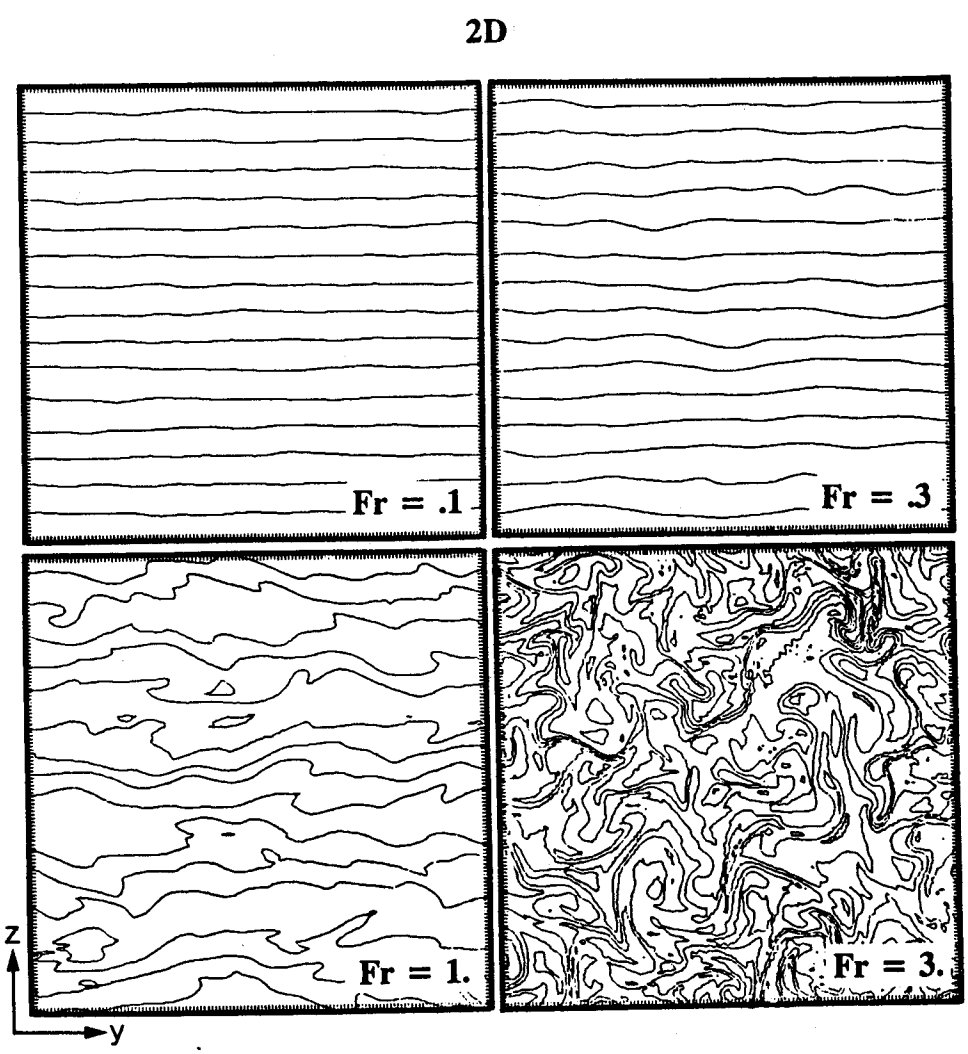

Figure 1b: Same as Figure 1a for 2D cases.

Table 1. Reynold's numbers and box sizes for the basic simulations

Froude number	3D Reynold's number	3D box size (m)	2D box size (m)
0.1	27.6	4.0	16.0
0.3	23.0	2.4	11.2
1	16.6	1.3	5.3
3	16.8	0.75	3.0

Nonlinear Energy Transfers

For the 3D dynamics, the nonlinear transfer of kinetic and potential energies can be expressed in the Fourier domain as:

$$\partial_t KE(k_h, k_z) = \mathbf{u}_\mathbf{k}^* \cdot (\mathbf{\Lambda} \times \mathbf{u})_\mathbf{k} \tag{13}$$

and

$$\partial_t PE(k_h, k_z) = -\rho_\mathbf{k}^* (\mathbf{u} \cdot \nabla \rho)_\mathbf{k} \tag{14}$$

where * denotes complex conjugation and the transfers are collected as functions of horizontal and vertical wavenumbers k_h and k_z. This formulation is helpful in revealing details of the nonlinear processes.

In 2D, the nonlinear transfer rates can be written in the Fourier domain as:

$$\partial_t KE(k_y, k_z) = \psi_\mathbf{k}^* \{J(\psi, \zeta)\}_\mathbf{k} - U_\mathbf{k}^* \{J(\psi, U)\}_\mathbf{k} \tag{15}$$

and

$$\partial_t PE(k_y, k_z) = -\rho_\mathbf{k}^* \{J(\psi, \rho)\}_\mathbf{k} \tag{16}$$

where the horizontal wavenumber is now k_y.

By averaging over many buoyancy periods, the energy transfer rates have been calculated. Figure 2 shows contours of these energy transfer rates for the case of Froude number 1. The 3D nonlinear transfer rates are contoured as a function of horizontal and vertical wavenumber, k_h and k_z and the 2D as a function of k_y and k_z. Areas which are losing energy due to nonlinear interactions have dashed contours and areas which are receiving energy have solid contours. The contour increments are logarithmic with a minimum energy cutoff of 1.0×10^{-3} times the maximum value. In order to emphasize those wavenumbers which are contributing significantly to the overall energy transfer, areas which receive/lose more than 10% of the maximum energy transfer rate are shaded.

For the 2D case, the kinetic energy may be divided into two parts, one which will be called 'planar' ('KeP' $\equiv \frac{1}{2} \sum_k k^2 |\psi|^2$) and the 'cross' energy ('KeC' $\equiv \frac{1}{2} \sum_k |U|^2$). PE is simply $\frac{1}{2} \sum_k |\rho|^2$. In Figure 2, both planar and U energy transfer rates are combined, hence it does not resemble a classical 2D energy transfer shape. For 3D, the distribution of KE and PE transfers are of similar shape and magnitude. For 2D, KE and PE distributions have somewhat dissimilar shapes, but the rates are again of comparable magnitude even though there is about twice as much kinetic energy as potential for all cases. The transfer of kinetic energy to small scales relative to potential energy appears suppressed in both 3D and 2D. A tentative exploration into the reasons for the similarity in net nonlinear transfer rates between 3D and 2D is presented in the section on Waves and Vortices.

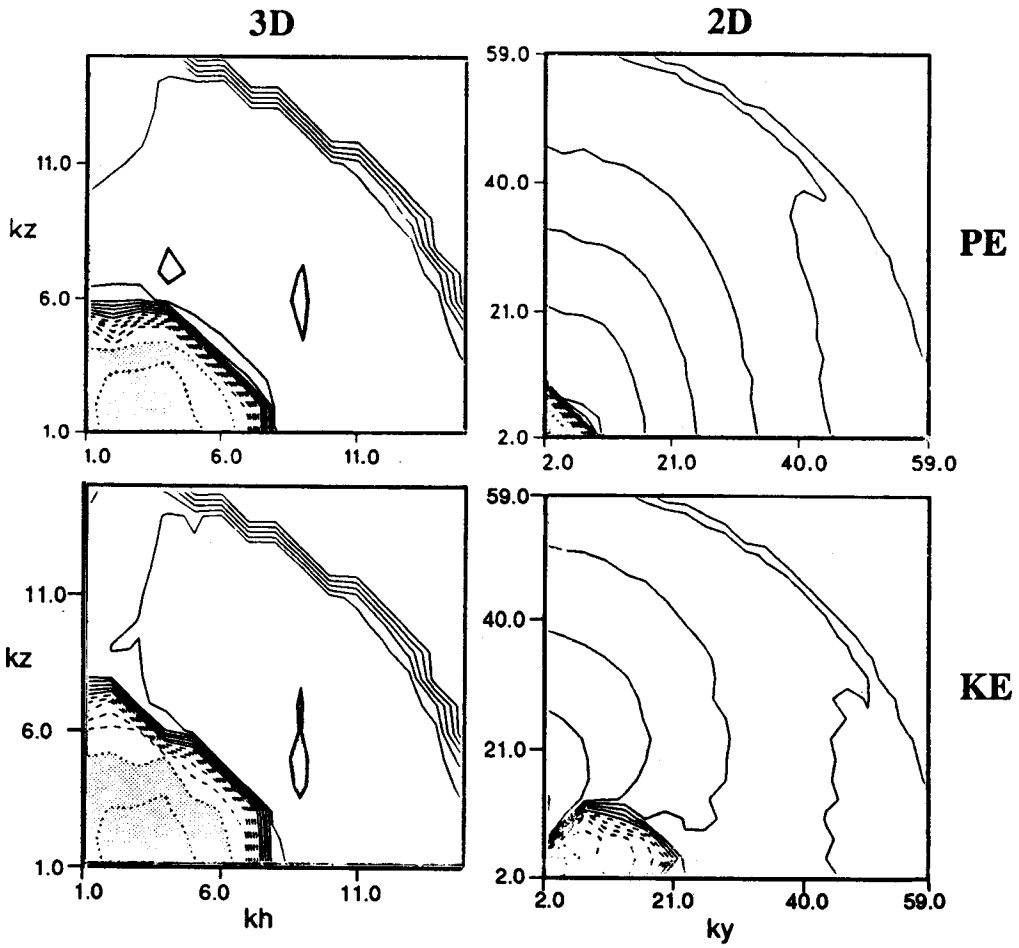

Figure 2: The net sums of potential (top) and kinetic (bottom) nonlinear transfers of energy for 3D (left) and 2D (right) both at a Froude number of 1 plotted versus horizontal and vertical wavenumbers. The logarithmic contour increments for Figures 2 and 4 are 0.71×10^{-4} for the 3D and 0.11×10^{-4} for the 2D with energy loss denoted by dashed contours and energy gain denoted by solid contours. The maximum transfer rates are 0.22×10^{-3} and 0.33×10^{-4} for 3D and 2D respectively. Areas which receive or lose more than 10% of the maximum are shaded.

Figure 3 shows the resultant energy spectra. The 3 cases presented are (Fr=0.3,f=0), (Fr=1, f=0) and (Fr=1,f=0.1). The 3D spectra are kinetic energy and twice potential energy. The 2D spectra are planar and cross kinetic energy and potential energy. For the 2D nonrotating cases, PE and planar KE would overlay exactly for a linear internal wave regime in energy equipartition. The departure from equipartition due to the nonlinear transfers is seen for the Froude number 1 case. The effect of rotation is to bring the 2D planar and U energy together with PE still greater than planar KE at the smallest scales.

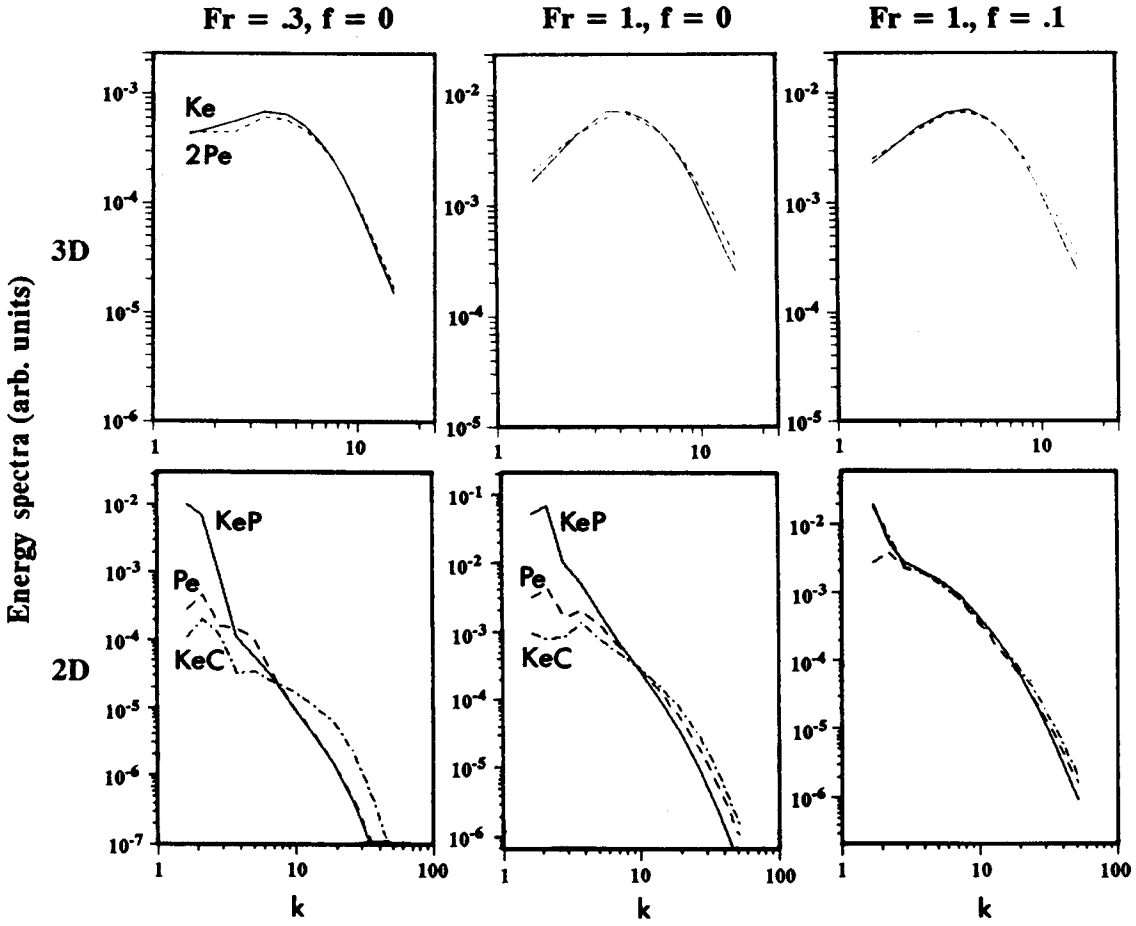

Figure 3: The 3D (top) and 2D (bottom) energy spectra for (left to right) Fr=0.3 f=0, Fr=1, f=0 and Fr=1, f=0.1 plotted versus total wavenumber. The 3D cases show kinetic (solid) and twice potential (dashed) energies. The 2D show planar (solid) and U (dashed) kinetic and potential ("Pe": dotted) energies.

For all the 3D cases, the tendency to produce an excess of potential energy relative to kinetic energy at the smallest scales (>1:2) is clearly seen with rotation having no discernible effect. For both 3D and 2D, the tendency is therefore to produce an excess of potential energy relative to kinetic energy at the smallest scales. For all cases shown in Figure 3, the low wavenumber regions have excesses of kinetic energy relative to potential energy. *Herring et al* [1982] have seen similar implications for eddy Prandtl numbers in closure models of passive scalar advection.

Figure 4 shows the buoyancy flux cross spectrum $-\langle \rho_{\mathbf{k}}^* W_{\mathbf{k}} \rangle$ for the same case shown in Figure 2. Time-averaged contours of this quantity are presented in the same manner as Figure 2. In both 3D and 2D, the shape of the time averaged buoyancy flux contours are negative (KE to PE conversion) at large scales and positive (PE to KE conversion) at small scales near the $k_z = 0$ axis. This shape can be interpreted as a direct result of the non-equipartition spectra seen in Figure 3.

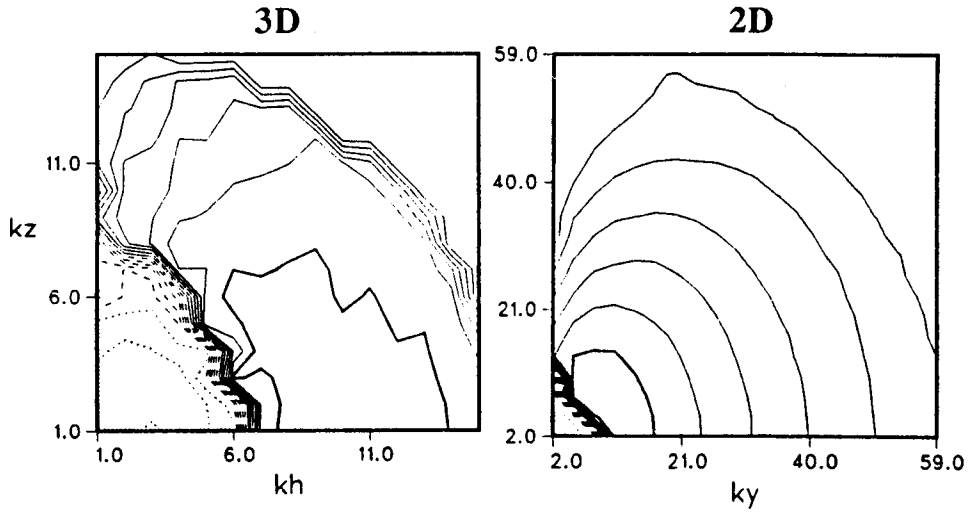

Figure 4: The buoyancy flux cross spectra from the same cases as Figure 2. The logarithmic contour increment for 3D (left) is 0.14×10^{-4} with a maximum of 0.44×10^{-4} and for 2D the increment is 0.32×10^{-5} with a maximum of 0.10×10^{-4}.

Figure 5 shows that all 3D cases have buoyancy spectra with this shape except for the weakest flow regime. *Shen and Holloway* [1986] show similar results for 2D which can also be inferred from Figure 4. *Holloway* [1988] has shown 2D spectral closure theory and simulations which take as the force term for buoyancy flux the difference between kinetic and potential energy. These yield buoyancy flux spectra not unlike those of Figure 5.

On Figure 5, the *Thorpe* [1977] overturning and buoyancy $\left(\sqrt{\epsilon/N^3}\right)$ scales have been marked where possible. Where a buoyancy scale has not been marked, it is at a scale less than the smallest available to the model. Since we have not defined 'patches' of overturning as observationalists would do, we have estimated the largest (Thorpe) scales of overturning as three times the calculated Thorpe scales. It is seen from Figure 5 that scales of mixing (negative buoyancy flux) are larger than either the Thorpe or buoyancy (where turbulence begins to dominate buoyancy) scales. The implication of this is that 'mixing' does not occur where overturning occurs, rather it occurs at the larger scales . Restratification appears to be happening at overturning scales. Kraig Winters critically addressed issues about the interpretation of mixing showing that a reordering of the ρ profile may be necessary to diagnose mixing. The reader should consider results described in the present paper from the view of *Winters* [1991].

Table 2 shows the time averaged net buoyancy fluxes, standard deviation of same and kinetic energy dissipation rate for the full range of 3D and 2D cases shown in Figure 1. As Table 2 shows, net buoyancy fluxes are on average not significantly different from zero for most 3D and 2D cases with or without rotation for these forcing ratios.

Only at a Froude number significantly greater than unity is there net negative buoyancy flux (destratification). Small amounts of overturning at a Froude number of 1 are not sufficient to

Table 2. Average net buoyancy fluxes and KE dissipation rates. All have f=0 unless noted.

Froude number	3D buoyancy flux	Standard deviation	ε	2D buoyancy flux	Standard deviation	ε
0.1	0.19 e-5	0.14 e-4	0.19 e-4	-0.25 e-6	0.14 e-4	0.13 3-5
0.3	0.15 e-4	-0.11 e-3	0.56 e-3	0.62 e-5	0.12 e-3	0.24 e-4
1	-0.47 e-4	0.11 e-2	0.25 e-1	0.15 e-3	0.16 e-2	0.16 e-2
1, f=0.1	-0.64 e-4	0.11 e-2	0.26 e-1	0.29 e-4	0.16 e-2	0.17 e-2
3	-0.20 e-1	0.13 e-1	0.73	-0.33 e-1	0.37 e-1	0.11

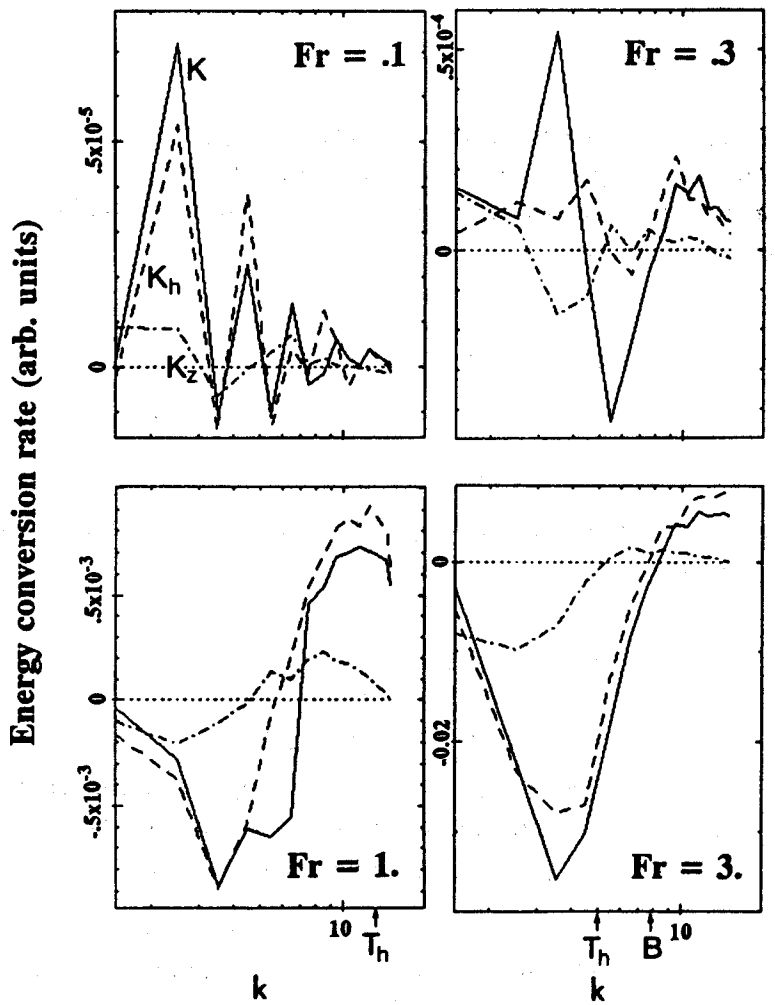

Figure 5: The 3D buoyancy flux cross spectra plotted versus total (solid), horizontal (dashed) and vertical (dot-dash) wavenumber for the 4 Froude number cases. The Thorpe and buoyancy scales are marked where possible.

cause net destratification in either 3D or 2D. A scaling of buoyancy flux from dissipation rate ($\rho' w' = 0.2\epsilon$, see *Osborne and Cox* [1972]) is only possible for one of the cases shown in Table 2 (2D, Froude number 3.). Obviously, the results are dependent on the ratio of forcing of KE:PE. *Moum* [1989] has reported directly measured values from overturning patches of $\rho'\omega' = 50$ W m^{-2}; $0.2\varepsilon = 420$ W m^{-2}. Moum cautions against taking these values too literally, but they are like the average values seen in the simulations using the energy equipartition rates of forcing.

The tendency to produce positive buoyancy fluxes at the high wavenumber end of an inertial subrange is very robust to the form of forcing. *Holloway and Ramsden* [1988] show a case without rotation which was run with forcing of kinetic energy only with correspondingly large negative net buoyancy fluxes. Even though the forced scales are very close to the Kolmogorov scale, a positive buoyancy flux 'tail' was observed. Other examples of this robustness are given in the same paper.

WAVES AND VORTICES

An attempt has been made to understand why 3D kinetic energy transfer is suppressed relative to potential energy by separating nonlinear transfers into component parts, viz: if all nonlinear, dissipative, and forcing terms are omitted from the 3D equations of motion then the ideal linearized model equations become

$$\partial_t \mathbf{u_k} = \frac{\mathbf{k}}{|k|^2}[k_z \rho_\mathbf{k} - f(k_x V_\mathbf{k} - k_y U_\mathbf{k})] - \rho_\mathbf{k}\mathbf{e_z} + f(V_\mathbf{k}\mathbf{e_x} - U_\mathbf{k}\mathbf{e_y}) \tag{17}$$

$$\partial_t \rho_k = -W_\mathbf{k} \tag{18}$$

The resultant system of equations (details may be found in RH) has eigenvalues zero and $\pm\frac{1}{|k|}\sqrt{k_h^2 + f^2 k_z^2}$ with corresponding eigenvectors

$$\begin{bmatrix} a_0 \\ a_+ \\ a_- \end{bmatrix} = \begin{bmatrix} 1/c & 0 & 1 \\ -c & d & 1 \\ -c & -d & 1 \end{bmatrix} \begin{bmatrix} v_c \\ v_a \\ \rho_\mathbf{k} \end{bmatrix} \tag{19}$$

with $c = f\frac{k_z}{k_h}$, $d = \iota\sqrt{1+c^2}$ and v_c, v_a are velocity components orthogonal to k. The a_0 is the nonpropagating vortical mode and $a_\pm$ are wave modes propagating at frequencies $\pm\frac{1}{|k|}\sqrt{k_h^2 + f^2 k_z^2}$. The 2D system possesses a similar set of solutions.

Note that the right hand sides of equations (13) and (14) are the product of three quantities, each of which is the sum of waves and vortices. Eight contributions to the net nonlinear transfers are thus possible. These are denoted by, *e.g.*, W-W-V where the interaction of waves and vortices is projected onto the wave component of the flow field. V-W-W would be wave-wave interactions projected onto the vortical part of the flow field. The 2D has a similar decomposition.

Examination of these transfer components have shown that for the 3D case the forward transfer of potential energy to small scales is matched by a corresponding kinetic energy transfer mode with the following notable exception. Figure 6 shows the kinetic and potential energy W-W-W interactions for both 3D and 2D to the same scale as Figure 2. This transfer mode appears to be the key player in the suppression of 3D KE transfers (at least for wave energy). The rate of energy transfer is *much* greater for potential energy than kinetic energy for *both* 3D and 2D and the shapes are the same, too. The point of this section is to isolate in some degree where the suppression of KE transfer relative to PE transfer is occurring and to reemphasize the similarity of 3D and 2D results.

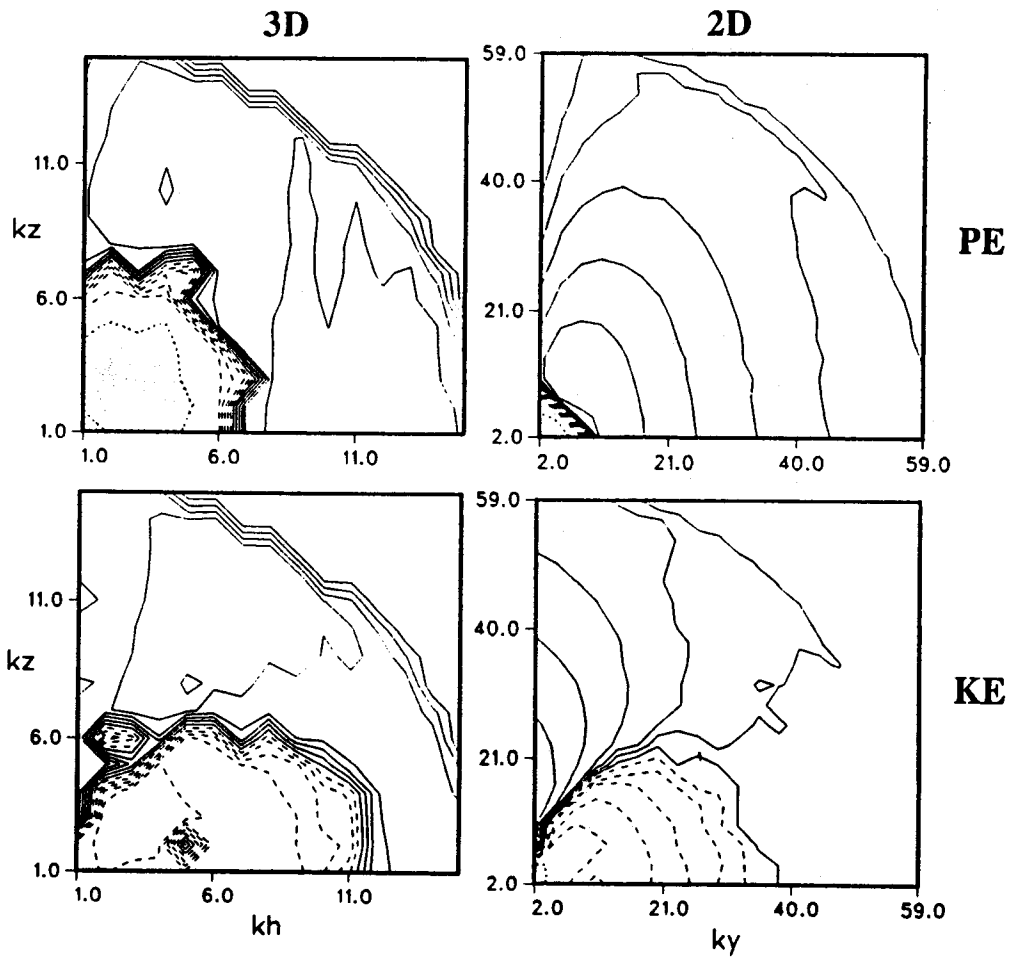

Figure 6: The W-W-W transfer component potential (top) and kinetic (bottom) energy transfers for 3D (left) and 2D (right) plotted versus vertical and horizontal wavenumbers. The scaling is as Figure 2.

CONCLUSIONS TO Part 1

The nonlinear transfer of kinetic and potential energy in an internal wave regime near dissipation scales has been investigated by direct numerical simulations. Two cases were considered, one which solves the full 3D Navier-Stokes equations and another which restricts the motion field to a vertical 2D plane. It was found that the rate of transfer of kinetic energy is less than that of potential energy for both 3D and 2D and the net transfer rates have similar spectral shapes. Although suppression of the 2D kinetic energy transfer is explained by the energy/enstrophy conservation restraint, the reason for KE suppression in 3D is not well understood.

The difference of transfer rate of KE and PE creates an imbalance in the relative amounts of kinetic and potential energies at different scales, more PE at small scales and more KE at the larger scales. The relative excesses of energy in turn drive a characteristic buoyancy flux spectrum, negative at large scales and positive at small scales, with the results from 2D resembling those of 3D. The tendency to produce a relative excess of potential energy at the high wavenumber end of an inertial range, resulting in positive (restratifying) buoyancy fluxes, is robust to the form of the forcing.

Rotation up to f=0.1 slightly alters the form of the 2D energy spectra but does not significantly affect the differential transfer rates leading to the buoyancy flux measurements. Rotation to f=0.1 has little effect on the 3D results due to the short energy residence times.

Net buoyancy fluxes are on average zero except at Froude numbers much larger than 1. There is little net mixing in a marginally overturning environment, either in 3D or 2D. An Osborne-Cox scaling to derive buoyancy flux from kinetic energy dissipation rates appears to be only possible in the most active of turbulent patches for the forcing ratios used here.

It may seem surprising that 2D dynamics resemble so nearly the full 3D regime with respect to the nonlinear behavior of internal waves near dissipation scales. It is encouraging to think that cost-effective numerical experiments in 2D may be relevant to real-world applications.

Part 2: SURFACE LAYER FORCING

One may criticize Part 1 apart from the extremely limited flow domain. Energy 'appears' by application of fictitious body forces which are intended to represent interactions with scales larger than the resolvable domain. Energy introduced at internal wave equipartition levels is moved to different scales by nonlinear processes, but no energy is created or destroyed by this process. Hence, it is perhaps not unexpected that the observed net buoyancy fluxes were small.

Holloway, [1988], [1989] has raised the issue that presumptions about gradient production and dissipation rates such as that of *Osborne and Cox* [1972] may be on shaky theoretical grounds. In order to gain insight into the relative strengths of terms in the Navier-Stokes equations, we have attempted to measure them in a simulation domain with a vertical flow of energy.

METHOD

The 2D simulation code used in Part 1 has been modified to have a free slip, rigid lid condition on ψ and ρ at grid resolution 128*256 (and preliminary 128*512). The forcing function has been masked by

$$M(z) = e^{-(\frac{3}{2}z)^2} \; ; -\pi < z < 0 \tag{20}$$

where the simulation domain is $-\pi < z < 0$. At each timestep, ψ and ρ have been multiplied by a bottom absorption taper function

$$T(z) = 1 - C\{1 - \left(10\left[1 + \frac{z}{\pi}\right]\right)^2\} \; ; -\pi < z < -0.9\pi \tag{21}$$

with C a constant.

In this way, it was attempted to define an 'energy radiation' region between the forced region and the sponge region which mimics the passage of energy down the fluid column. To simplify the energetics, the 'cross' velocity field has been eliminated (no rotation). Figures 7a and 7b show instantaneous snapshots of stream function, density and kinetic+potential energy density for one of the cases. It is seen that energy is concentrated in the 'surface' layer.

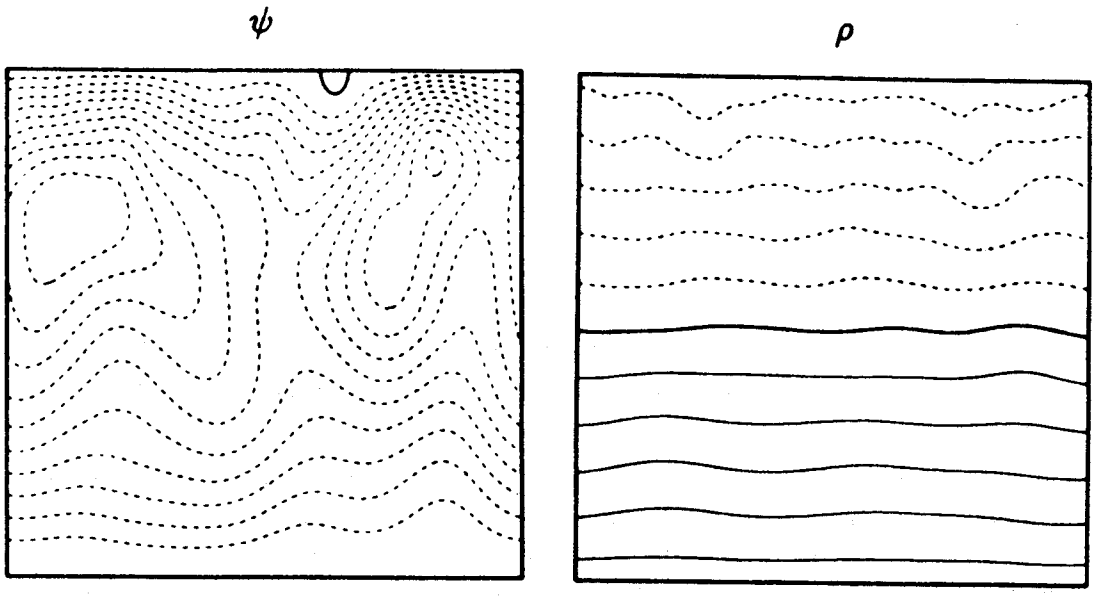

Figure 7a: Instantaneous snapshots of (left) stream function and (right) total density for a surface layer forced run.

Figure 8 shows vertical profiles of kinetic and potential energy and energy dissipation rates. It is seen that the presence of the sponge region creates gradients near the bottom which tend to enhance the dissipation rates, and there is probably some reflection of energy from the bottom.

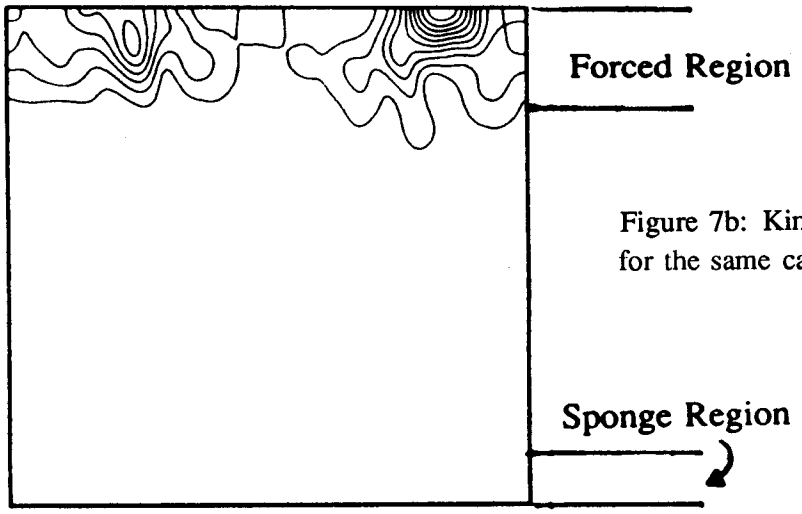

Figure 7b: Kinetic + potential energy density for the same case as Figure 7a.

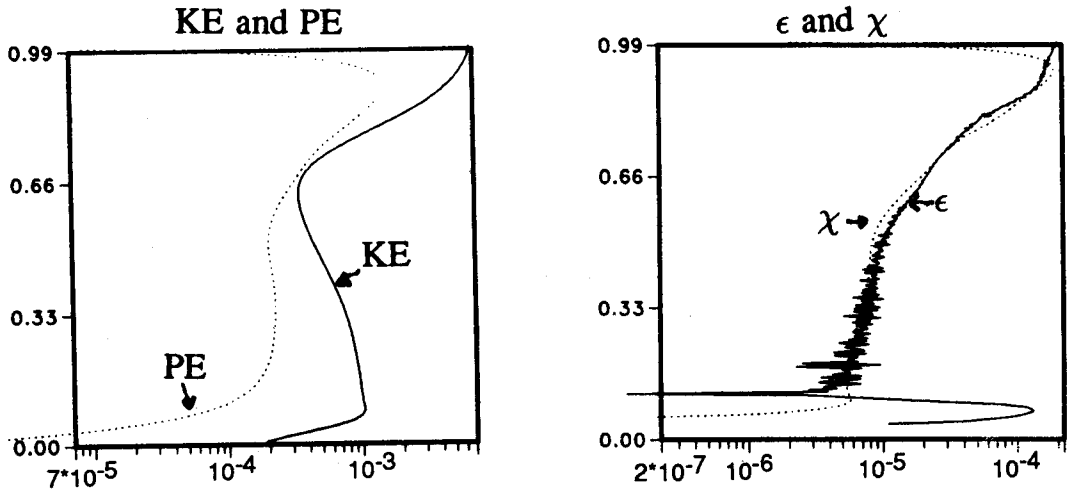

Figure 8: Time and horizontally averaged vertical profiles of (left) kinetic (solid) and potential (dotted) energy and (right) dissipation rates of kinetic (solid) and potential (dotted) energy.

Figure 9 shows energy spectra for the area away from the forced and sponged region only and a vertical profile of Froude number. The reduced area spectra indicate that there is more KE than PE away from the surface layer. This conclusion is supported by Figure 10, a vertical profile of buoyancy flux and a spectrum of buoyancy flux away from the mixed layer. For this case the net buoyancy flux is clearly negative in the radiation region but the spectrum is showing the tendency to develop a positive 'tail' as was seen in the homogeneously forced cases.

Nonlinear Energy Radiation Terms

In the radiation region, what are the sources and sinks of energy? We have attempted to answer this question by determining an energy balance in the non-forced region. From equation (1)

$$\partial_t(\mathbf{u}^2/2) = \nabla \cdot (\mathbf{u}p + \mathbf{u}\mathbf{u}^2/2) - \rho W - \epsilon \qquad (22)$$

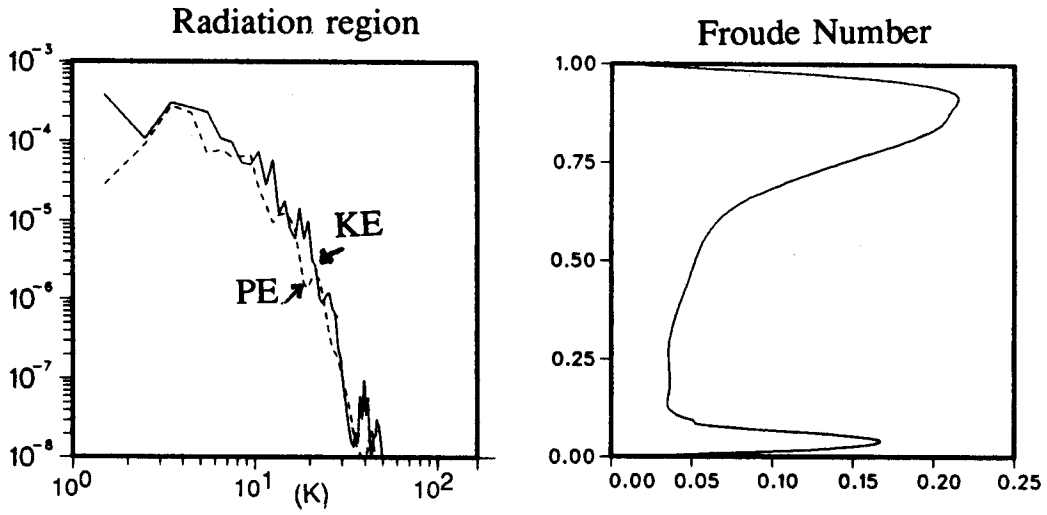

Figure 9: (left) Time averaged kinetic (solid) and potential (dashed) energy spectra plotted versus total wavenumber for radiation region only: (right) vertical profile of Froude number.

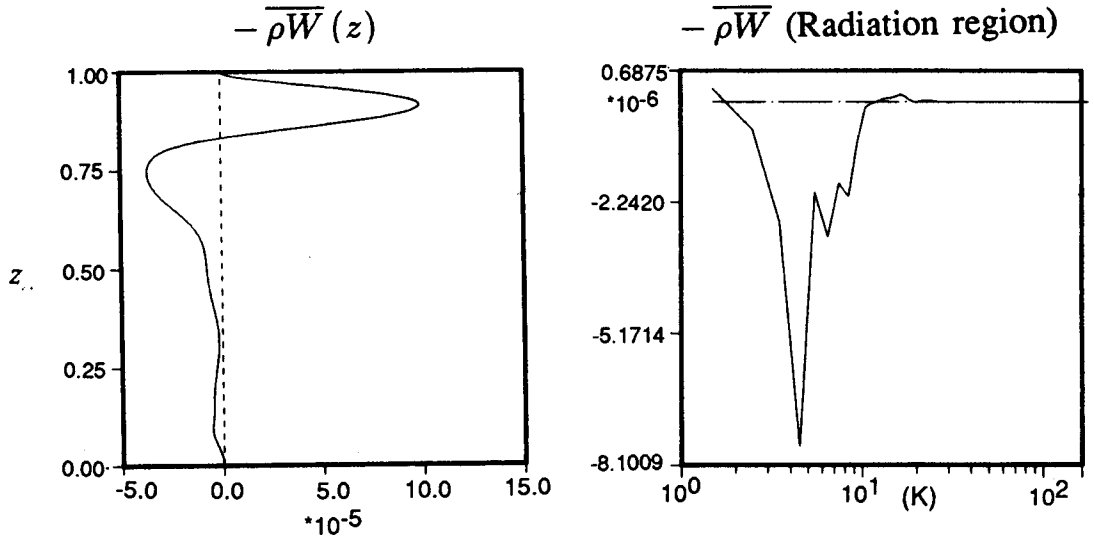

Figure 10: (left) Time and horizontally averaged profile of buoyancy flux; (right) time averaged buoyancy flux spectra from the radiation region plotted versus total wavenumber.

The nonlinear terms are composed of a divergence of a pressure-u correlation which we denote as 'up' and a turbulent flux term which we denote as 'tf'. The ρW is minus buoyancy flux and ϵ is kinetic energy dissipation rate. From equation (2)

$$\partial_t(\rho^2/2) = \nabla \cdot (\mathrm{u}\rho^2/2) + \rho W - \chi \tag{23}$$

where χ is potential energy dissipation rate and we will denote the nonlinear term as 'nl'.

Assuming that stationarity has been reached and the ∂_t terms can be dropped, which of the remaining terms in equations (22) and (23) are dominant? Figure 11 left shows vertical profiles of time and horizontally averaged 'nl', 'up' and 'tf' and Figure 11 right shows sums of terms for KE and PE. Clearly, it is the divergence of the pressure-u correlation which carries (kinetic) energy down the water column. Figure 11 right indicates a qualitative balance between nonlinear production, buoyancy flux and dissipation in the radiation region for both kinetic and potential energy (forcing and sponge region effects were not factored into the balances).

At level z=-π/2 in the radiation region, the average values of balance terms for two r.m.s Froude numbers are presented in Tables 3a and 3b. Table 3b indicates that the major source of potential energy in the radiation region is the buoyancy flux and the nonlinear term tends to remove potential energy. Table 3a and 3b indicate that buoyancy flux is of comparable magnitude to ϵ or χ (which are about equal).

$$tf \equiv \nabla \cdot (\mathbf{u}u^2/2)$$

$$up \equiv \nabla \cdot (\mathbf{u}p)$$

$$nl \equiv \nabla \cdot (\mathbf{u}\rho^2/2)$$

$$nl + \overline{\rho W} - \chi = 0?$$

$$tf + up - \overline{\rho W} - \epsilon = 0?$$

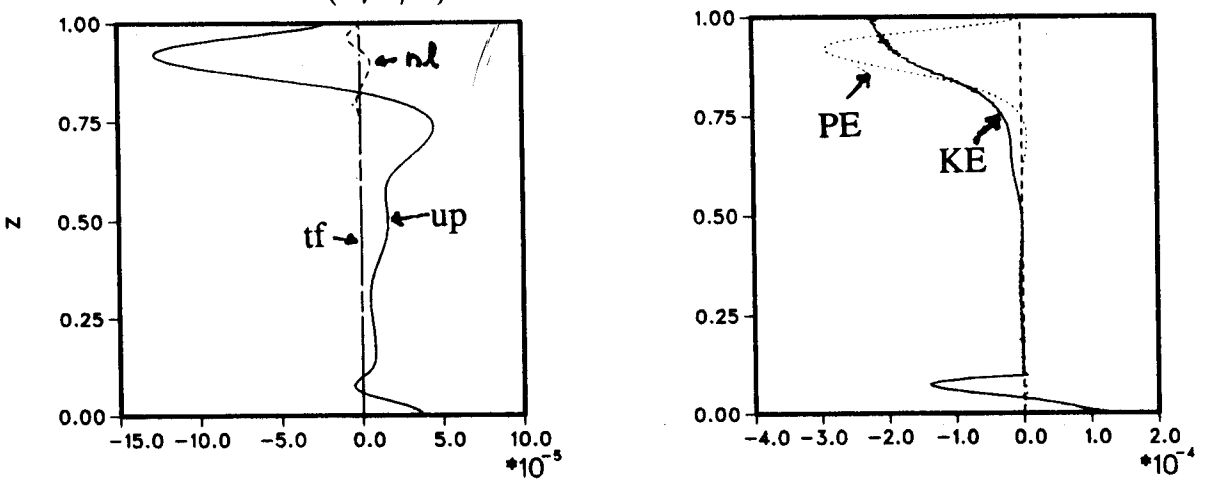

Figure 11: (left) Time averaged profiles of divergence of pressure-u correlation (solid), $\mathbf{u}u^2/2$ (dotted, not visible) and $u\rho^2/2$ (dashed). (Right) Time and horizontally averaged profiles of kinetic (solid) and potential (dotted) energy balance sums along with the terms which go into the sums.

CONCLUSIONS TO Part 2

For the cases studied here, energy from the surface forced layer moves down the fluid column by the pressure-u correlation. The turbulent flux term in the equations of motion is negligible compared to the divergence of the pressure-u correlation. The kinetic energy supplied to the fluid interior is balanced by dissipation and conversion to potential energy via buoyancy flux. The buoyancy flux is hence on average negative in the radiation region, but the spectrum

Table 3a. Kinetic energy balance terms.

Froude number	up	tf	b*w	ε	sum
0.05	0.17 e-4	-0.46 e-10	-0.74 e-5	-0.11 e-4	-0.165 e-5
0.15	0.44 e-4	-0.93 e-8	-0.22 e-4	-0.13 e-4	0.85 e-5

Table 3b. Potential energy balance terms

Froude number	nl	-b*w	χ	sum
0.05	-0.24 e-7	0.74 e-5	-0.84 e-5	-0.11 e-5
0.15	-0.18 e-5	0.22 e-4	-0.15 e-4	0.51 e-5

shows the same qualitative behavior (negative at large scales, positive at small scales) as the statistically homogeneous forced cases.

The major source of potential energy in the fluid interior is the buoyancy flux and it is roughly balanced by dissipation and (relatively small) vertical nonlinear transfer. Taken together, Parts 1 and 2 indicate the hazard of scaling buoyancy flux rates from dissipation rates. Indication is that net buoyancy flux occurs during times in which energy is 'filling' a region. When energy levels reach sufficient magnitude to cause a dissipation 'event', there may be very little net gradient flux associated with it, but this may have little to do with 'mixing' (again *Winters* [1991]). Future work will concern attempting to extend the parameter range to higher Froude number radiation regions and completing runs at the higher resolution (larger radiation region).

ACKNOWLEDGMENTS

The assistance of Patricia Kimber in drafting the figures is gratefully acknowledged. This work was supported in part by the Office of Naval Research under grant number N00014–87–J-1262.

REFERENCES

Crawford, W., A Comparison of Length Scales and Decay Times of Turbulence in Stably Stratified Fluids, *J. Phys. Ocean.*, 16, 1847–1854, 1987.

Gargett, A., P. Hendricks, T. B. Sanford, T. R. Osborn and A. J. Williams III, A Composite Spectrum of Vertical Shear in the Upper Ocean, *J. Phys. Oceanogr.*, **11**, 1258–1271, 1981.

Herring, J. R., D. Schertzer, M. Lesieur, G. R. Newman, J. P. Chollet and M. Larchevsque, A Comparative Assessment of Spectral Closures as Applied to Passive Scalar Diffusion, *J. Fluid. Mech.*, **124**, 411–437, 1982.

Holloway, G., A Conjecture Relating Oceanic Internal Waves and Small-Scale Processes, *Atmos. Ocean*, **21**, 107–122, 1983.

Holloway, G., The Buoyancy Flux from Internal Gravity Wave Breaking, *Dyn. Atmos. Oceans*, **12**, 107–125, 1988.

Holloway, G., Relating Turbulence Dissipation Measurements to Ocean Mixing, Proc. 'Aha Huliko'a Hawaiian Winter Workshop, ed. P. Muller and D. Henderson, Hawaii Inst. of Geophys., 329–339, 1989.

Holloway, G., and D. Ramsden, Theories of Internal Wave Interaction and Stably Stratified Turbulence: Testing Against Direct Numerical Experimentation, in Small-Scale Turbulence and Mixing in the Ocean, J. C. H. Nihoul and B. M. Jamart eds., Elsevier, 363–378, 1988.

Moum, J. N. , Measuring Turbulent Fluxes in the Ocean, the Quest for K_ρ, Proc. 'Aha Huliko'a Hawaiian Winter Workshop, ed. P. Muller and D. Henderson, Hawaii Inst. of Geophys., 145–156, 1989.

Muller, P., R-C. Lien and R. Williams, Estimates of Potential Vorticity at Small Scales in the Ocean, *J. Phys. Oceanogr.*, **18**, 401–416, 1988.

Orszag, S. A., Numerical Simulation of Incompressible Flows Within Simple Boundaries. I. Galerkin (spectral) Representations, *Stud. in Appl. Math.*, 50, 293–297, 1971.

Osborne, T. R. and C. S. Cox, Oceanic Fine Structure, *Geophys. Fluid Dyn.*, 3, 321–345, 1972.

Ramsden, D. and G. Holloway, Direct Simulation and Turbulence Closure Evaluation for Large Amplitude Internal Wave Interactions in the Vertical Plane, *Proc. of Third Intl. Sympos. on Stratified Flows*, Cal. Inst. of Technology, Vol. 1, 1987.

Ramsden, D. and G. Holloway, Energy Transfers across an Internal Wave/Gravity Mode Spectrum, preprint, 1990.

Riley, J., R. W. Metcalfe, and M. A. Weissman, Direct Numerical Simulations of Homogeneous Turbulence in Density stratified Flows, in Nonlinear Properties of Internal Waves, AIP Conf. Proc. No. 76, 79–112, 1981.

Robert, A., The Interpretation of a Low Order Spectral Form of the Primitive Meteorological Equations, *J. Met. Soc. of Japan*, 44, 237–244, 1966.

Shen, C. Y., and G. Holloway, A Numerical Study of the Frequency and Energetics of Nonlinear Internal Gravity Waves, *J. Geophys. Res.*, 91, C1, 953–973, 1986.

Thorpe, S. A., Turbulence and Mixing in a Scottish Loch, *Phil. Trans. Roy. Soc. London*, A286, 125–181, 1977.

Winters, K., Diagnosing Mixing in Numerical Models, Proc. 'Aha Huliko'a Hawaiian Winter Workshop, ed. P. Muller and D. Henderson, Hawaii Inst. of Geophys., in press, 1991.